TRANSIENT FINITE-DIFFERENCE TSUNAMI CALCULATIONS

Ove Skovgaard[1] and Ivar G. Jonsson[2]

ABSTRACT

The applicability of a time-stepping approximate finite difference method is tested for the response of a plane incoming tsunami of small amplitude meeting an idealized island (see Fig 1). The resulting amplitudes are compared with the exact solution, which comes out of solving the linear shallow water wave equation for the area in question. Since this wave equation excludes dissipation (bottom friction) and the Coriolis force, these terms are omitted in the Boussinesq equations, formulated as mass and momentum conservation, which are the bases of the finite difference scheme. Grid size is 1 × 1 km. The incoming wave is time-harmonic with a period of T = 480 s; the (test) solution to the wave equation is thus a truly steady-state solution. The finite difference scheme, however, has a so-called "cold start" and so it is transient in principle. During a time corresponding to three periods, in which disturbances from the open boundaries still have only a small effect on the wave field near the island, the time-series of signals in selected points can define a steady response, though. Considering the inevitable shortcomings of a provisional study like the present, satisfactory agreement with the exact solution is met over the shoal in Fig 1. We have thus a promising starting point for more elaborate studies, comprising new filtering algorithms for the boundaries, tests with real transient input signals, and including non-linearity, bottom friction, and the Coriolis force.

The numerical scheme used is the so-called System 21, developed at the Danish Hydraulic Institute and placed at our disposal for the present study.

1. INTRODUCTION

A seismic sea wave, a so-called tsunami (Japanese for "harbour wave"), consists of a series of waves that approaches the coast with periods usually ranging from 5 to 90 min (Murty, 1977, p 2). The length of these waves is of the order of hundreds of kilometres in the deep ocean, while here their amplitude is usually of the order of a metre. They are therefore difficult to detect from the air or from ships. Near land, however, the tsunami will build up in height due to the decrease in water depth.

---

[1] Associate Professor, Laboratory of Applied Mathematical Physics (LAMF), Bldg 303, Technical University of Denmark, DK-2800 Lyngby.

[2] Associate Professor, Institute of Hydrodynamics and Hydraulic Engineering (ISVA), Bldg 115, same address.

At the same time the amplitude can be further amplified because of lateral convergence and reflections. The wave length will be reduced in shallower water.

The final run-up of tsunamis is a highly non-linear phenomenon. In this preliminary report of our study, however, we shall investigate the modification of the tsunami wave over that area near the coast, where linear theory can be used, ie excluding the final run-up.

A tsunami can also be generated by non-seismic causes, such as landslides and nuclear explosions. Therefore Murty (1977, p 1) cites the more general definition by van Dorn: "Tsunami is the Japanese name for the gravity wave system formed in the sea following any large-scale, short-duration disturbance of the free surface." Most of the current knowledge about tsunamis is excellently reviewed in the above-mentioned book by T S Murty.

We will calculate the transformation of a small, time-harmonic, and plane incident wave caused by an idealized island of circular cylindrical form, situated on a paraboloidal shoal in an infinite ocean of constant depth, see Fig 1.

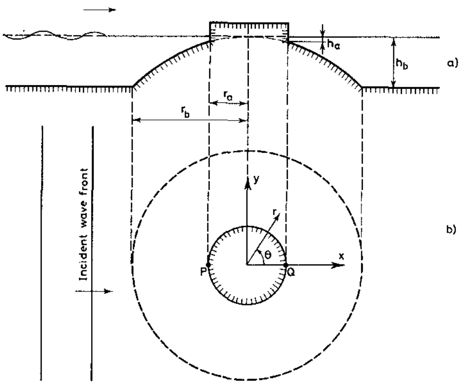

Fig 1. Sketch of the idealized island on a paraboloidal shoal;
a) vertical, b) horizontal.

The water depths h are

$$h = \alpha r^2 \qquad \text{for } r_a \le r \le r_b \quad \text{and} \quad 0^\circ \le \theta < 360^\circ$$
$$h = h_b \; (= \alpha r_b^2) \qquad \text{for } r_b \le r < \infty \quad \text{and} \quad 0^\circ \le \theta < 360^\circ \tag{1.1}$$

Shoreline radius is r_a = 10 km, outer radius of shoal is r_b = 30 km, and depth h_b = 4,000 m. Thus shoreline depth is $h_a = h_b (r_a/r_b)^2$ = 4,000/9 ≈ 444 m. (Generally subscript a denotes a value at the shoreline, and subscript b denotes a value at the outer boundary of the shoal.) The factor of proportionality α in (1.1) becomes $\alpha = 4/9 \times 10^{-5}\ m^{-1}$.

This type of island is seemingly accepted as being representative of a "Pacific island" (Homma, 1950). Experiments have been performed by Williams and Kartha (1969).

The present paper is a sequel to papers by Jonsson et al (1976) (hereafter referred to as paper I), where we restricted the presentation to the wave field at the shoreline, including some shallow water refraction calculations, and by Jonsson and Skovgaard (1979) (hereafter referred to as paper II), where we looked at the wave field over the shoal for wave periods up to 240 s, including a few intermediate depth refraction calculations for the shoreline.

The purpose of the present paper is twofold. Firstly to investigate the exact wave field (amplitudes and phase angles) outside the shoal, ie to study the "disturbance" out in the deep ocean due to the presence of the island. Secondly, we will use a finite difference (FD) method (FD in space and time) to see how accurate such an approximate solution is in a small region around the island and the shoal. For both cases the diffraction contours will be determined corresponding to small, time-harmonic and plane incident waves, and only for one wave period T = 480 s. This period is above the shallow water limit for the island, which for $h/L = 1/20$ gives $T \approx 410$ s. Notice that for larger islands T = 480 s corresponds to a greater period (fixed ratio between wave length L and radius).

Earlier FD approaches for tsunami wave problems are described by Camfield (1980), and finite-element (FE) methods for such problems are reviewed in Sklarz et al (1979).

Tsunami waves are basically transient, but we have performed this preliminary study with "unphysical" periodic waves in order to assess the feasibility of transient FD models for "small" regions with long open boundaries. Our ultimate goal is to test the FD model for a short transient Gaussian-like pulse, where we can also construct the "exact" test solution, by superposition of time-harmonic exact solutions.

2. ASSUMPTIONS AND DEFINITIONS

The incident surface gravity waves are assumed to be plane, time-harmonic, and of small amplitude. The Coriolis force is neglected, which is justified for the considered higher end of the tsunami frequency range. The island sides are assumed fully reflecting. Non-linear effects (including dissipation) will be neglected, although they can easily be included in the approximate solution, see Sect 4.

The diffraction of simple time-harmonic and very long surface gravity waves (in practice $h/L < 0.05$) over a gently sloping sea bed is governed by the linearized long-wave equation

$$\nabla \cdot (h \nabla \eta) + h k^2 \eta = 0 \qquad (2.1)$$

where ∇ is the horizontal gradient operator $(\partial/\partial x, \partial/\partial y)$ or $(\partial/\partial r, r^{-1}\partial/\partial\theta)$, $k = 2\pi/L$ is the wave number, $L = cT$ is the wave length, c is the phase speed (2.6), $h = h(r,\theta)$ the water depth, and $\eta = \eta(r,\theta)$ is the (complex) surface wave amplitude. r and θ are defined in Fig 1.

Note that the instantaneous complex surface elevation is $\eta \exp(-i\omega t)$, where i is the imaginary unit, $\omega = 2\pi/T$ is the (constant) angular frequency, and t is time. The instantaneous real surface elevation ζ is thus

$$\zeta = \mathrm{Re}\,\{\eta\,\exp(-i\omega t)\} \tag{2.2}$$

We define the real surface amplitude $A = A(r,\theta)$ and phase angle $\varphi = \varphi(r,\theta)$ (also real) by

$$\eta = A\,\exp(i\varphi) \tag{2.3}$$

ie we have from (2.2)

$$\zeta = A\,\cos(\varphi - \omega t) \tag{2.4}$$

Phase angle φ is still determined less an arbitrary constant. This is remedied by demanding that φ be zero in the far field at $\theta = \pm 90^\circ$ for $t = 0$. In other words, φ is the phase angle at that instant, when the undisturbed wave crest passes through the centre of the island.

The real amplitude of the incoming wave is called A_i. In the amplitude graphs we have depicted the relative amplitudes A/A_i.

The incident waves have the surface elevation

$$\zeta_i = A_i\,\cos(kx - \omega t) \tag{2.5}$$

For very long waves there is no dispersion and the phase and group speeds (c and c_g) are equal and given by

$$c = c_g = \sqrt{gh} \tag{2.6}$$

in which g is the gravity acceleration.

For calculations involving (2.1) we use the acronym SWT which stands for Shallow Water Theory.

Equation (2.1) is correct to first order in both wave amplitude and bed slope, see eg Jonsson and Brink-Kjær (1973).

The diffraction of mildly non-linear surface gravity waves (transient or periodic) over a gently sloping sea bed is governed by the Boussinesq equations, in which the vertical velocity is supposed to increase linearly from zero at the bed to a maximum at the surface, in two horizontal space variables and time. The Boussinesq equations are formulated as mass and momentum conservation laws (integrated over depth). In terms of volume discharge or depth-integrated velocities the governing equations read (see Abbott et al, 1978, p 177, (4) - (6)):

$$\frac{\partial \zeta}{\partial t} + \frac{\partial p}{\partial x} + \frac{\partial q}{\partial y} = 0 \tag{2.7}$$

$$\frac{\partial p}{\partial t} + \frac{\partial}{\partial x}\left(\frac{p^2}{h^*}\right) + \frac{\partial}{\partial y}\left(\frac{pq}{h^*}\right) + gh^*\frac{\partial \zeta}{\partial x} = \tfrac{1}{2}hh^*\left[\frac{\partial^3}{\partial x^2\partial t}\left(\frac{hp}{h^*}\right) + \frac{\partial^3}{\partial x\partial y\partial t}\left(\frac{hq}{h^*}\right)\right] - \tfrac{1}{6}h^2h^*\left[\frac{\partial^3}{\partial x^2\partial t}\left(\frac{p}{h^*}\right) + \frac{\partial^3}{\partial x\partial y\partial t}\left(\frac{q}{h^*}\right)\right] \tag{2.8}$$

$$\frac{\partial q}{\partial t} + \frac{\partial}{\partial y}\left(\frac{q^2}{h^*}\right) + \frac{\partial}{\partial x}\left(\frac{pq}{h^*}\right) + gh^*\frac{\partial \zeta}{\partial y} = \tfrac{1}{2}hh^*\left[\frac{\partial^3}{\partial y^2\partial t}\left(\frac{hq}{h^*}\right) + \frac{\partial^3}{\partial x\partial y\partial t}\left(\frac{hp}{h^*}\right)\right] - \tfrac{1}{6}h^2h^*\left[\frac{\partial^3}{\partial y^2\partial t}\left(\frac{q}{h^*}\right) + \frac{\partial^3}{\partial x\partial y\partial t}\left(\frac{p}{h^*}\right)\right] \tag{2.9}$$

where $h^* \equiv h + \zeta$, ie the instantaneous total depth, p is the x-component of the volume discharge, and q is the y-component of the volume discharge. x and y are defined in Fig 1. For the long, small amplitude waves considered in this preliminary study the third derivative terms (the right-hand sides) in (2.8) and (2.9) are almost negligible, as they represent the deviation of the pressure distribution from the hydrostatic pressure.

In (2.8) and (2.9) we have for the time being neglected the Coriolis force and dissipative effects (bottom friction).

3. THE EXACT SHALLOW WATER THEORY (SWT) SOLUTION

In order to calculate the total wave field in any point of the area we must solve the partial differential equation (2.1), the shallow water wave equation. The boundary conditions are full reflection at the island ($r = r_a$) and Sommerfeld's radiation condition at infinity (for the scattered part of the wave field). See paper I for details.

Because of the rotational symmetry of the bathymetry we can apply the method of separation of variables.

Over the shoal ($r_a \leq r \leq r_b$) the solution for the complex amplitude is

$$\eta = \sum_{n=0}^{\infty} R_n(r) \cos(n\theta) \qquad 0 \leq \theta < 360^\circ \tag{3.1}$$

where the functions $R_n(r)$, ($n = 0,1,2,\cdots$), are solutions to linear two-point boundary value problems. These ordinary differential equations were solved by Homma (1950), see paper I, pp 473-476, for details. Angle θ is defined in Fig 1.

Outside the shoal ($r \geq r_b$) the wave field is the sum of an incident and a scattered wave field, ie

$$\eta = \eta_i + \eta_{sc} \tag{3.2}$$

with η_i rewritten as

$$\eta_i = A_i \sum_{n=0}^{\infty} \varepsilon_n \, i^n J_n(k_b r) \cos(n\theta) \tag{3.3}$$

and

$$\eta_{sc} = \sum_{n=0}^{\infty} C_n H_n^{(1)} (k_b r) \cos(n\theta) \tag{3.4}$$

In these equations A_i is the amplitude (real) of the incoming wave, ε_n is the Neumann factor (ie $\varepsilon_n = 1$ for $n = 0$, and $\varepsilon_n = 2$ for $n \neq 0$), i is the imaginary unit, J_n are Bessel functions of nth order and first kind, $k_b = 2\pi/L_b$, the wave number for $r \geq r_b$, C_n are integration constants, and $H_n^{(1)}$ are Hankel functions of the nth order and first kind.

At $r = r_b$ there is continuity in η and in its first derivative with respect to r. Using the former condition we find from (3.1) and (3.2) for the determination of C_n

$$C_n = \frac{1}{H_n(\tau)}\left[(R_n)_{r=r_b} - A_i\,\varepsilon_n\, i^n\, J_n(\tau)\right] \qquad n = 0,1,2,\cdots \tag{3.5}$$

where we have dropped the superscript (1) on H, and further $\tau \equiv k_b\, r_b$. Functions $(R_n)_{r=r_b}$ are determined by Homma's (1950) solution (see (3.19) in paper I). Inserting the results in (3.5) yields

$$C_n = \frac{A_i \varepsilon_n i^n}{H_n}\left[\frac{i\left[\rho^{\alpha_n} - \frac{\alpha_n - 1}{\alpha_n + 1}\rho^{-\alpha_n}\right]\frac{2}{\pi}\rho^{\alpha_n}}{\rho^{2\alpha_n}\left[(1-\alpha_n)H_n + \tau H_n'\right] - \frac{\alpha_n - 1}{\alpha_n + 1}\left[\tau H_n' + (1+\alpha_n)H_n\right]} - J_n\right] \qquad n = 0,1,2,\cdots \tag{3.6}$$

where $\rho \equiv r_b/r_a$, $\alpha_n \equiv \sqrt{1+n^2-\tau^2}$, and we have dropped the argument τ of the Hankel function and its derivative (ie here $H_n' = (dH_n^{(1)}(k_b r)/d(k_b r))_{r=r_b}$).

The complete solution outside the shoal hereafter emerges from (3.2) - (3.4) with (3.6) inserted in the latter equation.

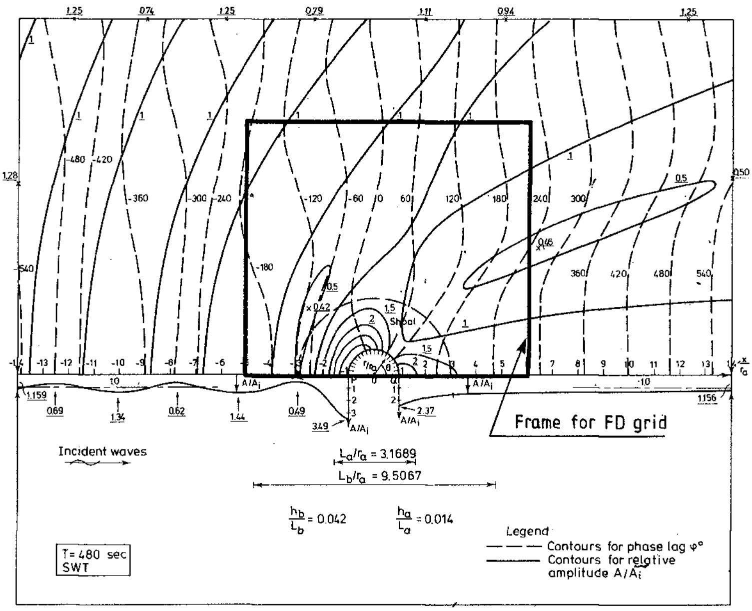

Fig 2. Contours for relative amplitude A/A_i and phase angle φ over the shoal and on constant water depth outside. Solution of (2.1) (ie SWT) for T = 480 s. The intervals between A/A_i-curves are 0.5 and between φ-curves they are 60^o. Underscored numbers are A/A_i. The rectangular frame (the very thick line) will be discussed in Sect 4.

A solution for T = 480 s is depicted in Fig 2 showing contours for relative amplitude A/A_i and phase lag φ^o over the shoal and on constant water depth outside. The solution is presented for $|x/r_a| \leq 14$ and $y/r_a \leq 14$. Maxima and minima are indicated along the boundaries of the depicted area. It appears that even some wave lengths away from the island the incident wave is quite perturbed. A similar figure to Fig 2 has been constructed for a smaller wave period (T = 240 s), see Skovgaard and Jonsson (1980), Fig 2.

An important application of the very accurate ("exact") solution in this section is that it can serve as a check for more general numerical schemes (see Sect 4). In order to facilitate such a check a test solution is tabulated in Table 1. In the table relative amplitude A/A_i and phase angle φ are given for one period (T = 480 s), for seven values of azimuth θ (= 0^o, 30^o, 60^o, 90^o, 120^o, 150^o, and 180^o), and for four values of relative distance, r/r_a (= 1, 3, 9, and 27). The table is an extension of paper I, Table 2a, which stopped at the base of the shoal (r/r_a = 3). Also another period is chosen here, T = 480 s, instead of T = 410.47••• s.

For the practical application of the finite Fourier series for the diffraction solution (3.1) or (3.2) to (3.4) it is useful to know how many terms one needs in order to obtain a given accuracy. This information can be even more important when we discuss whether a certain solution approach at all can be applied in a certain period range or in a certain space region of r and θ.

In paper I (3.24) we introduced the number of terms n_{max} necessary to obtain a prescribed relative accuracy eps (0 < eps << 1), which we here define by the relation

$$\left| \sum_{n=0}^{n_{max}} R_n(r) \cos (n\theta) - \text{exact solution} \right| < \text{eps} \times A_i \tag{3.7}$$

or

$$\left| (A/A_i)_{\text{approximate}} - (A/A_i)_{\text{exact}} \right| < \text{eps} \tag{3.8}$$

This simple accuracy criterion, which directly controls the amplitudes and neglects the phases, is selected because of its simplicity. The exact solutions to (3.1) or (3.2) to (3.4) were constructed by continuing the summation until the last term of $|R_n/A_i|$ was less than eps squared.

In Fig 3 for T = 480 s (using the shallow water wave equation (2.1) and $\theta = 0^o$ (ie along the positive part of the x-axis) n_{max} vs x/r_a is shown for $1 \leq x/r_a \leq 28$ and for eps = 10^{-2}, 10^{-4}, and 10^{-8}. (eps = 10^{-d} is normally referred to as two times d-places decimal accuracy.)

Similar figures have been constructed for other values of θ, and from these figures we can conclude that Fig 3 is in practice valid for arbitrary θ. For a fixed r/r_a the difference between n_{max} in Fig 2 and the n_{max} in figures for other θ was never larger than 2.

The general conclusion is that n_{max} increases monotously with x/r_a. For eps constant the variation is nearly linear from the island and outwards. From Fig 3 we can further conclude that for points on the shoal, n_{max} is only increased by one or two (depending on eps) when we "move"

Table 1. Diffraction solution for the wave field over the shoal, and on constant water depth. The values of phase angle φ are chosen in the interval $0^{\circ} \le \varphi < 360^{\circ}$. Integers in parentheses indicate powers of 10 by which the following numbers are to be multiplied.

Using SWT, (2.1), T = 480 s.

	$\theta = 0^{\circ}$	$\theta = 30^{\circ}$	$\theta = 60^{\circ}$	$\theta = 90^{\circ}$	$\theta = 120^{\circ}$	$\theta = 150^{\circ}$	$\theta = 180^{\circ}$
$(A/A_i)_{r=r_a}$	2.3692	1.7783	1.5253	2.6996	3.4019	3.5147	3.4886
$(\varphi^{\circ})_{r=r_a}$	(+2)1.4971	(+2)1.3245	(+1)5.9653	(+1)1.5667	(+2)3.5518	(+2)3.4112	(+2)3.3548
$(A/A_i)_{r=3r_a}$	1.5321	1.0055	(-1)8.0589	1.3347	(-1)9.9241	(-1)5.1496	(-1)4.9201
$(\varphi^{\circ})_{r=3r_a}$	(+2)1.9384	(+2)1.7399	(+1)7.0596	(+1)2.0287	(+2)3.4407	(+2)2.8704	(+2)2.4844
$(A/A_i)_{r=9r_a}$	1.2252	(-1)5.7584	1.0596	(-1)9.6740	1.1041	(-1)7.7372	1.0993
$(\varphi^{\circ})_{r=9r_a}$	(+1)2.6548	(+2)3.3426	(+2)1.6076	(+2)3.4795	(+2)2.0800	(+1)4.6236	(-1)2.2356
$(A/A_i)_{r=27r_a}$	1.0872	(-1)8.3750	1.0067	(-1)8.9622	1.1868	1.1405	(-1)7.9512
$(\varphi^{\circ})_{r=27r_a}$	(+2)3.2973	(+2)1.4407	(+2)1.4437	(+2)3.5730	(+2)2.1209	(+2)2.0341	(+1)5.2146

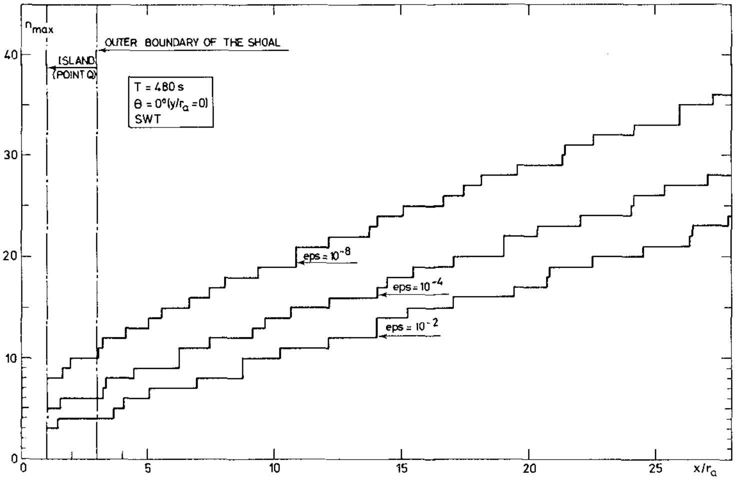

Fig 3. The necessary number of terms n_{max} in the Fourier series (SWT solution) vs x/r_a for $T = 480$ s, $1 \le x/r_a \le 28$ (℄ of shadow region), and eps $\doteq 10^{-2}$, 10^{-4}, and 10^{-8}.

from the island to the outer boundary of the shoal. If eps is decreased from 10^{-2} to 10^{-4} only up to five additional terms are needed in the solution series for x/r_a less than 28 and for $T = 480$ s (Fig 3). If eps is again squared (ie eps = 10^{-8}) only up to seven additional terms are needed. (Notice that for $\theta = 0^{\circ}$ all the $\cos(n\theta)$ factors in (3.7) are equal to one.)

Similar figures to Fig 3 have been constructed for other values of wave period T and from these figures we have found that if we use x/L (instead of x/r_a) as abscissa, Fig 3 becomes in practice valid for an arbitrary SWT wave period (or wave length L):

Inspection of the calculated phases revealed that the approximation errors for these basicly followed the same dependence on wave period T and on the horizontal coordinates r and θ as depicted for A/A_i in Fig 3.

The conclusion is that n_{max} increases with decreasing period (shorter waves). Far away from the island the increase is rapid. We can further summarize that for all periods in the SWT range, and for all points as far as at a distance of, say $r/r_a \approx 10$, only up to 20 terms of the series solution are needed for eps $\gtrsim 10^{-4}$. As far as at a distance of, say $r/r_a \approx 30$ only up to 40 terms are needed for eps $\gtrsim 10^{-4}$. For solutions in any point on the shoal only up to eight terms are needed in the SWT period range for eps $\gtrsim 10^{-4}$.

4. THE FINITE-DIFFERENCE (FD) SOLUTION

The time-dependent vertically integrated mass and momentum equations (2.7) - (2.9) are approximated by a third order alternating direction implicit (ADI) finite difference (FD) method with space- and time-staggered grids. The program or the modelling system (known as System 21) is described in detail in Abbott et al (1978) and (1979).

The program is designed primarily to cover physical situations with relatively short open boundaries, in contrast to the island cases, where we have radiation out of the computational area along all outer boundaries. For given incident waves the program allows the radiated waves to pass through the open boundaries, assuming that the radiated and the incident waves are of small amplitude and are propagating perpendicularly to the boundary. In the tsunami cases with isolated islands, the open boundaries are normally situated over the deeper part of the oceans where the waves in practice fulfil the first assumption (small amplitude).

The second assumption (waves propagating perpendicularly to the opening) can be well fulfilled in for instance a harbour resonance study. This has been demonstrated in a number of cases, some of which were reported by Abbott et al (1978). In the present case, however, the assumption can at best be approximately fulfilled at some of the boundaries, and the computations will give errors in the computed surface elevations at the open boundaries. These errors will have the appearance of waves reflected from the open boundaries into the region under investigation. If the reflected waves have a large angle of incidence at a physical open boundary the best one can do with the present system is probably to close the boundary in question and put a strong dissipation over a few grid lines along it, thereby simulating that most of the wave energy which enters the boundary region is radiated out. Another - much more expensive - possibility is to make the computational area so large that reflection from "critical" boundaries is delayed sufficiently. It is immediately seen from Fig 2 that the top boundary is the most critical one. See also Sect 6.

The open boundaries mean that we have exposed the system to quite a nasty test, trying to reproduce the solution in Sect 3 using time-stepping calculations. The input wave in the FD system is time-harmonic, but as the calculations are started from a so-called "cold state" they are transient in principle.

The island with the shoal and a fraction of the surrounding ocean (the area within the thick frame in Fig 2) has been covered by a grid, see Fig 4. The grid spacing Δx and Δy is the same in both directions. Δx or Δy denotes the distance between two consecutive grid points for the water level or for the bathymetry; due to the staggered grid the distance between the flux grid points and the elevation grid points is $\frac{1}{2}(\Delta x)$ in the x-direction and $\frac{1}{2}(\Delta y)$ in the y-direction. In this paper we have used only one grid-size ($\Delta x = \Delta y = 1$ km) and only one frame, which covers an area of (109×99) km^2, or 110 grid points ($J = 0,1,\cdots,109$) in the x-direction and 100 grid points ($K = 0,1,\cdots,99$) in the y-direction, see Fig 4. The model is closed along the symmetry line (x-axis), here $K = \frac{1}{2}\Delta y$. The model is open along $J = 0$, where we prescribe a given time-harmonic "incident" surface elevation of small amplitude. Similarly the model is open along $J = 109$, where we prescribe an "incident" wave of

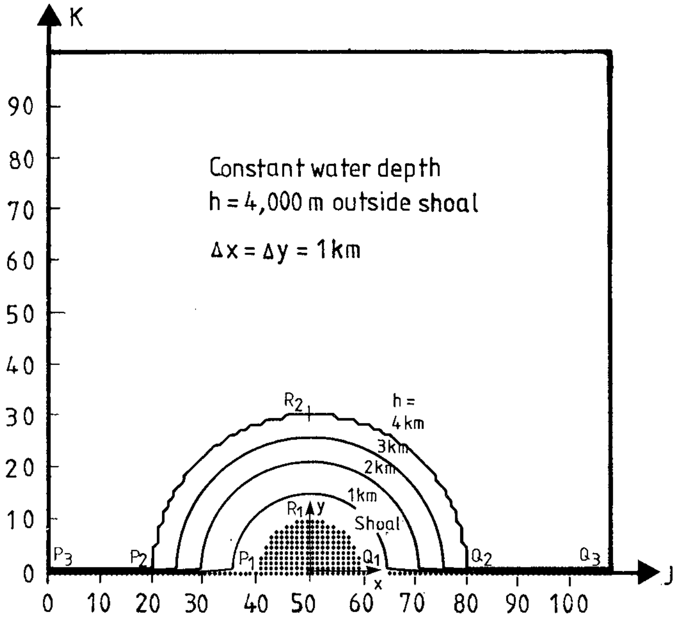

Fig 4. The numerical model bathymetry of the area within the thick frame in Fig 2. The intervals between the depth contours are 1 km. The coordinates for P_1, P_2, P_3, Q_1, Q_2, Q_3, R_1, and R_2 are defined in Table 2.

zero amplitude. Along K = 99 (the most critical boundary) we have closed the model and put some dissipation along the boundary. The origin O of the x-y coordinates in Fig 1 (centre of the island) has the coordinates (J,K) = $(50\frac{1}{2}, \frac{1}{2})$.

Due to the simple rectangular discretization of the island (see Fig 4) and to a smaller extent of the shoal we can only get an approximation of the diffraction pattern over the shoal, especially so at the shoreline.

The most direct representation of the solution is time-series plots of relative surface elevations (ie calculated surface elevations divided by A_i, see (2.5)) in characteristic points of the modelled area. We have selected eight such points (P_1, P_2, P_3, Q_1, Q_2, Q_3, R_1, and R_2), see Fig 4 and Table 2. The eight relative surface elevations are given in Figs 5, 6, 7, and 8 for the one incident wave period tested, T = 480 s.

In this provisional stage of the project we have run the model only a rather short time, viz three wave periods or 3 × 480 s = 1440 s. This integration time was determined by an estimate of the propagation time for a small disturbance entering the model at P_3 (see Fig 4), travelling along the negative x-axis to point P (see Fig 1), continuing along the border of the island to the y-axis, further along the y-axis up to the

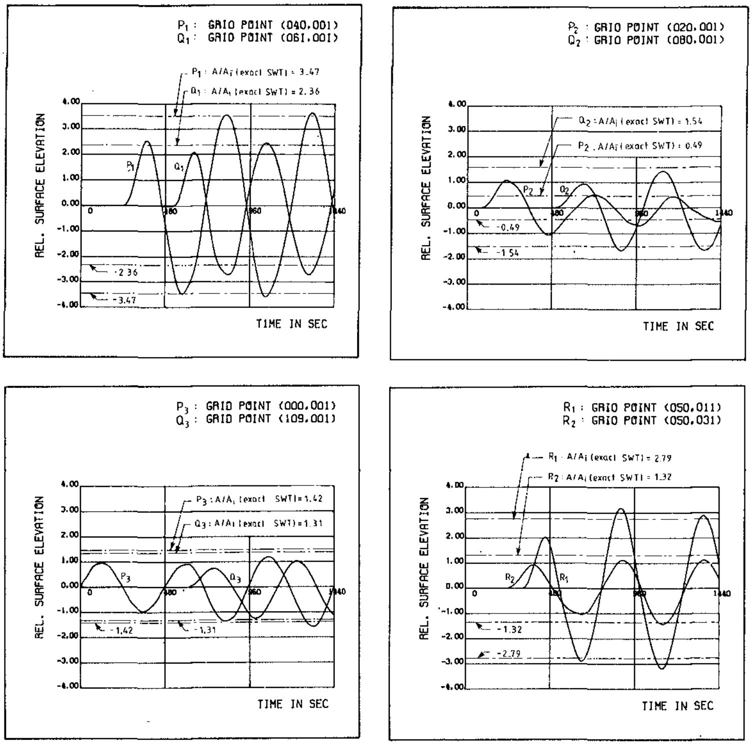

Figs 5 - 6 - 7 - 8. Relative surface elevation vs time t ($0 \leq t \leq 1440s = 3 \times 480$ s) for 8 points (P_1, P_2, P_3, Q_1, Q_2, Q_3, R_1, and R_2) within the FD grid, see Fig 4. Period is $T = 480$ s. Exact max/min SWT values of A/A_i from Sect 3 also shown.

most critical "closed" dissipative boundary and back to the outer boundary of the shoal. Using SWT (2.6) this travel time can be estimated as

$$t_s = \int \frac{ds}{c} = \frac{20,000 + 2 \times 68,000}{\sqrt{9.80665 \times 4000}} + \frac{2 \times \ln 3}{\sqrt{9.80665 \times 4/9 \times 10^{-5}}} + \frac{\frac{1}{2}\pi \times 10,000}{\sqrt{9.80665 \times 444.4\cdots}} \tag{4.1}$$

$$t_s \approx 788 + 333 + 238 = \underline{1359 \text{ s}} \ . \tag{4.2}$$

s being a local coordinate along the travel path for the disturbance. If the disturbance is allowed to travel further from the outer boundary of the shoal to the island (along the y-axis) we have $t_s \approx 1359 + 166 = 1525$ s.

	P_1	P_2	P_3	Q_1	Q_2	Q_3	R_1	R_2
J	40	20	0	61	80	109	50	50
K	1	1	1	1	1	1	11	31
x/r_a	-1.05	-3.05	-5.05	1.05	2.95	5.95	-0.05	-0.05
y/r_a	0.05	0.05	0.05	0.05	0.05	0.05	1.05	3.05

Table 2. Coordinates for the points P_1, P_2, P_3, Q_1, Q_2, Q_3, R_1, and R_2 in Fig 4.

We can conclude that for $t_s = 1440$ s ($= 3 \times 480$ s) the wave field over the shoal cannot be seriously distorted by our "crude" closing of the boundary along K = 99. On the other hand we must admit that the complete time-harmonic diffraction pattern over the shoal has not reached an equilibrium state within the three wave periods we have simulated, but it is promising to observe how close we come to the eight exact maximum/minimum SWT values of A/A_i from Sect 3. (To ensure linearity, which is assumed in the exact solutions, we have used a very small value of A_i.)

5. COMPARISON BETWEEN EXACT (SWT) AND APPROXIMATE (FD) SOLUTIONS

In the preceding section we compared in Figs 5 - 8 with the exact SWT values of A/A_i, for eight characteristic points within the FD frame in Figs 2 and 4. A more convincing approach is to compare the contours for the relative amplitude A/A_i from the exact (SWT) solution with the FD approximations. Details of the exact SWT wave field over the shoal and in its immediate vicinity are for T = 480 s presented in Fig 9 which is an enlarged version of the central part of Fig 2.

The contour lines in Fig 10 were found in the following way. All results from the FD calculations were stored on a file, and for $960 \text{ s} \le t \le 1440$ s (or $2 \times T \le t \le 3 \times T$) the maximum value ζ_{max} was found in each grid point and stored on a second file. For the same time interval the minimum value ζ_{min} was found in each grid point and stored on a third file. The relative amplitude A/A_i was then calculated in each grid point as $A/A_i \equiv \frac{1}{2}(\zeta_{max} - \zeta_{min})/A_i$ and stored on a fourth file. From the latter file the contour plot for A/A_i in Fig 10 was prepared, and A/A_i in 14 selected points along two half-circles ($r/r_a = 1.05$ and 3, $\theta^o = 0, 30, \cdots, 180$) was plotted against the exact SWT solution for $r/r_a = 1.05$ and 3, $0 \le \theta \le 180^o$, see Fig 11.

Remembering that in this provisional stage of the project we are interested only in the diffraction pattern over the shoal we can by comparison of Figs 9 and 10 (which are drawn to the same scale) conclude that the FD approximation is able to model all essential features of the diffraction pattern both in the illuminated region and in the shadow region.

If we look at the comparison in Fig 11 we notice an excellent agreement along the outer boundary of the shoal and a reasonably good agreement along the half-circle very near the island. It is natural that the crude discretization of the island will give the strongest modification very near the island and can be detected far less at the outer boundary of the shoal.

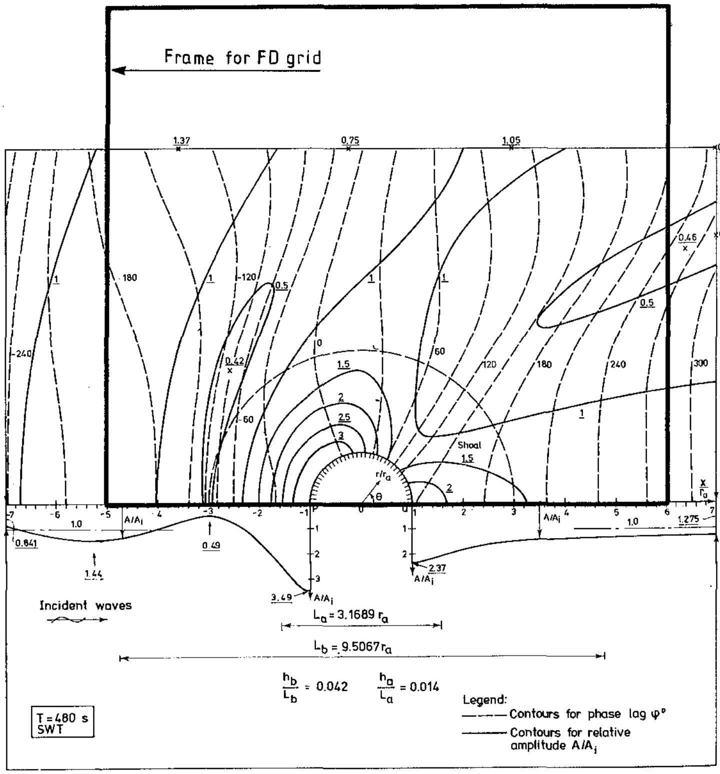

Fig 9. Contours for relative amplitude A/A_i and phase angle φ over the shoal and on constant water depth outside. Solution of (2.1) (ie SWT) for T = 480 s. The intervals between A/A_i-curves are 0.5 and between φ-curves they are 30°. Underscored numbers are A/A_i. The thick frame refers to the FD area covered in Fig 10, see also Fig 2.

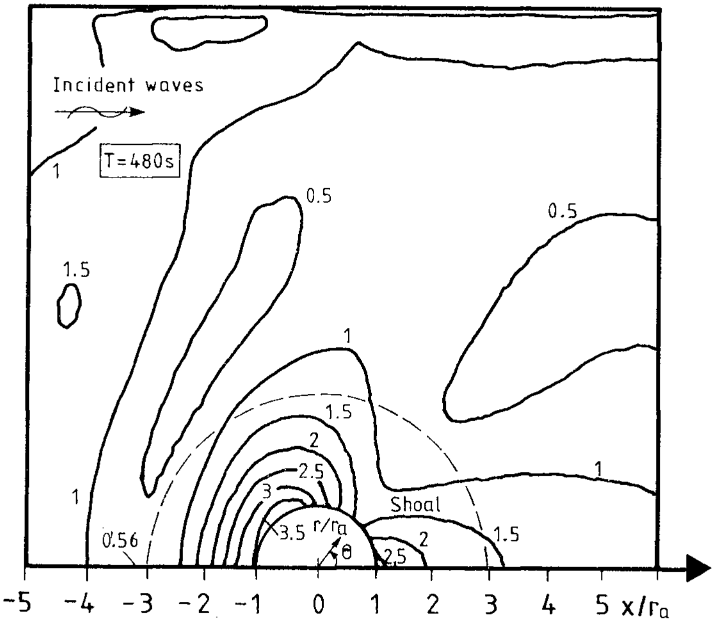

Fig 10. Contours for relative amplitude A/A_i over the shoal and on constant water depth outside. FD solution of (2.7 - 2.9) for periodic incident waves (T = 480 s) of small amplitude. The intervals between A/A_i-curves are 0.5. Same horizontal scale as in Fig 9.

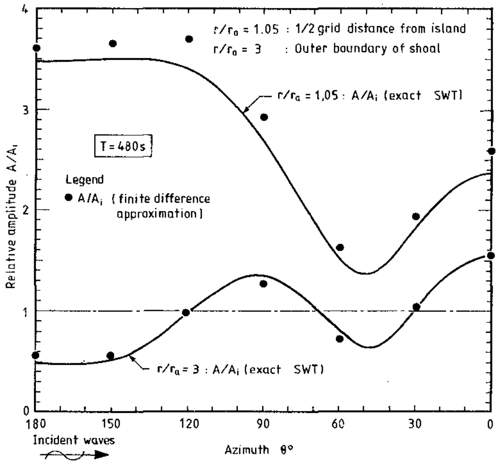

Fig 11. Relative amplitude A/A_i vs azimuth θ^o along two half-circles, r/r_a = 1.05 and 3. Full curves from exact solution of (2.1) (ie SWT) for T = 480 s, and dotted points from FD solution of (2.7 - 2.9) for periodic incident waves (T = 480 s) of small amplitude.

6. FUTURE WORK

In this preliminary study we have constructed and used the exact time-harmonic SWT solution (Sect 3) as reference solution for the periodic small amplitude approximate FD solution. In the subsequent more refined work we may construct and use the exact time-harmonic intermediate depth theory (IDT) solution (see Skovgaard and Jonsson (1980), Sect 3.2) as reference solution for the periodic small amplitude FD solution.

The FD model will be improved by construction and analysis of filtering algorithms which take account of the direction of the waves in relation to the boundary and which work for arbitrary Courant numbers $Cr \equiv c\Delta t/\Delta x$, Δt being the full time step in the FD-model.

We are also going to construct a more realistic "exact" test solution corresponding to a transient input (a Gaussian pulse, for instance). With this transient input we will expose the FD model to a more realistic test than the periodic test in this paper.

For this transient FD solution we will construct associated FD solutions which separately will include the Coriolis force and friction forces, thereby being able to show the effects of these two forces.

Finally the FD model will be used on some existing islands in the Pacific Ocean exposed to some "recorded" incident tsunami waves, thereby including the non-linear part of the FD model in the very shallow regions around the islands.

ACKNOWLEDGEMENTS

The Computational Hydraulic Centre, Danish Hydraulic Institute, is acknowledged for letting us use their versatile System 21 for the finite difference computations, including their many service programs.

The Joint Institute for Marine and Atmospheric Research (JIMAR), University of Hawaii, is acknowledged for the stimulating hospitality offered one of the authors (I.G. Jonsson) in the spring 1980 in connection with this study.

REFERENCES

Abbott, M B, H M Petersen, and O Skovgaard, 'On the numerical modelling of short waves in shallow water', J Hyd Res, 16, 3, 173-204, 1978.

Abbott, M B, H M Petersen, and O Skovgaard, 'Computations of short waves in shallow water', Proc 16th Coastal Engrg Conf, Aug-Sept 1978, Hamburg, Am Soc Civ Engrs, N Y, 1, 722-741, 1979.

Camfield, F E, 'Tsunami engineering', Special Rep No 6, U S Army Coastal Engrg Res Center, U S Government Printing Office, Washington, D C, p 222, 1980.

Homma, S, 'On the behaviour of seismic sea waves around circular island', Geophys Mag, 21, 3, 199-208, 1950.

Jonsson, I G, and O Brink-Kjær, 'A comparison between two reduced wave equations for gradually varying depth', Inst of Hydrodyn and Hydr Engng (ISVA), Tech Univ Denmark, Prog Rep No 31, 13-18, 1973.

Jonsson, I G, and O Skovgaard, 'A mild-slope wave equation and its application to tsunami calculations', Marine Geodesy, 2, 1, 41-58, 1979. (Paper II).

Jonsson, I G, O Skovgaard, and O Brink-Kjær, 'Diffraction and refraction calculations for waves incident on an island', J Mar Res, 34, 3, 469-496, 1976. (Paper I).

Murty, T S, 'Seismic sea waves. Tsunamis', Bull No 198, Dept of Fisheries and Marine Service, Scientific Information and Publications Branch, Ottawa, x + 337 + 41 pp, microfiche, 1977.

Sklarz, M A, L Q Spielvogel, and H G Loomis, 'Numerical simulation of the 29 November 1975 Island of Hawaii tsunami by the finite-element method', J Phys Oceanogr, 9, 5, 1022-1031, 1979.

Skovgaard, O, and I G Jonsson, 'Computation of wave fields in the ocean around an island', Danish Cent Appl Math & Mech (DCAMM), Tech Univ Denmark, Rep No 175, 67 pp, 1980.

Williams, J A, and T D K Kartha, 'Model study of long-wave amplification by circular islands', Bull Seism Soc America, 59, 1, 299-316, 1969.